Investigation of an Iterative Method for Finding of Currents, Voltages and Termination Impedances of PCB Traces Based on Phase-less Near-field Data

Robert Nowak
On-board Systems Lab
TU Dortmund University
Dortmund, Germany
robert.nowak@tu-dortmund.de

Stephan Frei
On-board Systems Lab
TU Dortmund University
Dortmund, Germany
stephan.frei@tu-dortmund.de

***Abstract*—The evaluation of near-field data can be an effective way to analyze EMI sources. In contrast to antenna measurements, near-field techniques can determine the emitted field without special requirements on the measurement environment. Moreover, critical sources can be found when current distributions can be identified. Therefore, current reconstruction methods for PCB traces were developed. With additional voltage information the termination impedances of the traces can be found. The known phase-less approaches suffers from different limitations, e.g., non-unique reconstruction results. In this paper, the necessary conditions for a unique reconstruction are discussed by investigating simulated phase-less near-field data. Based on these findings, measured near-field data of a PCB trace is evaluated, and the successful retrieval of the phase information is shown. Additionally, reconstructed voltage distributions are presented and compared to measurement data.**

Keywords—EMI, near-field, source reconstruction, iterative algorithm, phase retrieval, current reconstruction method.

I. Introduction

For the investigation of electromagnetic interference (EMI), several near-field techniques were developed and applied in the last years. In contrast to antenna measurements based on far-fields, near-field techniques can be used to estimate the field emission of a structure without the need of special measurement environments like an anechoic chamber. Mostly equivalent source models based on Huygens boxes [1], field integral equations [2], or dipole models [3] are used in these techniques. Moreover, there are near-field techniques to identify the critical field sources of a structure. For this purpose, [4] presents a method based on the plane-wave spectrum theory for the localization of sources. In contrast to [1]-[4], the evaluation of near-field data can also be supported by using geometry information of the investigated structure as shown in [5] where the currents are reconstructed. Here, the PCB trace system's current distribution is assumed as the field source. This method also yields information about the trace's terminations for selection of suppression measures.

While [1]-[4] require complex-valued near-field data, the approach presented in [5] evaluates phase-less data. However, this method cannot find an unambiguous solution. Therefore, one goal of this work is an extension of the current reconstruction method to obtain unique results by phase retrieval. Additionally, the potential of voltage amplitude and phase distribution reconstruction is discussed.

Several publications propose approaches to evaluate magnitude-only near-field data. On the one hand, there are direct methods that can retrieve phase information evaluating two (or more) field scan planes [6], [7]. However, these approaches demand very sensitive measurements on the distant planes. Therefore, additional scan planes are limited to strong emission sources. On the other hand, iterative methods can be used. Here, too, multiple scan planes can be evaluated for the retrieval of the phase [8]. However, in [9], an iterative approach based on a single scan plane is presented. As it needs regular gridded field data, measurement time can be very long. More preferable are current reconstruction methods based on arbitrarily selectable measurement points. Other iterative or evolutionary algorithms, as presented in [10] and [11], show improvements. However, as with other algorithms, different results are to be expected for different initial conditions. Wrong initial conditions can cause the methods to fail. The presented initial conditions seem to be chosen arbitrarily and optimized for the specific configuration. General rules for the appropriate selection are missing.

In this paper, the initial and the stop conditions of an iterative algorithm are discussed and advices for the proper selection are given. Based on these findings, the current reconstruction method is applied to the measured field data of a printed circuit board (PCB). In contrast to previous papers [5], [12]-[13], that analyzed only simplified structures, round wires in homogeneous media, here, we present results of the current reconstruction method for a PCB-trace on typical substrate (inhomogeneous media). Moreover, the reconstructed voltage distribution based on near-field data is also presented and compared to measurement data for the first time.

The geometry, wave impedances, and the propagation constants of the investigated PCB trace system are assumed to be known in this paper. In addition, perfect electric conducting infinite ground planes are assumed and losses are neglected.

The paper is structured as follows. In the next chapter, the current reconstruction method is summarized. Then, based on simulation data, the general investigation of conditions for a successful reconstruction is presented in chapter III. Afterward, an application example is shown, and reconstruction results based on measured field data are discussed. The paper closes with a conclusion and an outlook.

II. Current Reconstruction Method

In this section, the applied current reconstruction method for phase-less near-field data is summarized. Based on earlier works [5], [12], [13], the inverse problem, the used iterative algorithm, and the determination of voltage distribution are shortly summarized.

A. Formulation of the Inverse Problem

For the application of the current reconstruction method, the investigated PCB trace system is discretized into

segments, as shown in Fig. 1. Every segment carries a constant current. In this way, a discretized current distribution is formulated. All segment currents are concentrated in the vector $\mathbf{I}_\mathrm{S}$. As shown in [12], this vector, which can be very long, can be substituted by a vector with reduced length. For short sections of the trace like section k_1 in Fig. 1, a constant current distribution is assumed, and the segment currents are substituted by the current $I_{\mathrm{c,k}_1}$. At longer sections, such as section k_2 in Fig. 1, a current distribution defined by the transmission line theory is assumed. Thus, knowing the propagation constant γ_{k_2}, the segment currents of this section are substituted by the incident and reflected wave $I_{\mathrm{i,k}_2}$ and $I_{\mathrm{r,k}_2}$. Using these substitutions in $\mathbf{\Psi}_\mathrm{TL}$, $\mathbf{I}_\mathrm{S}$ is represented by the reduced current vector $\mathbf{I}$:

$$\mathbf{I}_\mathrm{S} = \underbrace{\begin{bmatrix} [1 \cdots 1]^\mathrm{T} & & \mathbf{0} \\ & \ddots & \\ \mathbf{0} & & \begin{bmatrix} \vdots & \vdots \\ \mathrm{e}^{-\gamma_{\mathrm{k}_2} d} & -\mathrm{e}^{\gamma_{\mathrm{k}_2} d} \\ \vdots & \vdots \end{bmatrix} \end{bmatrix}}_{=\mathbf{\Psi}_\mathrm{TL}} \cdot \underbrace{\begin{bmatrix} I_{\mathrm{c,k}_1} \\ \vdots \\ I_{\mathrm{i,k}_2} \\ I_{\mathrm{r,k}_2} \end{bmatrix}}_{=\mathbf{I}} . \tag{1}$$

In this formulation, d is the position of the centers of the segments in section k_2. In this way, the current distribution $\mathbf{I}_\mathrm{S}$ is completely represented by this reduced vector.

For every segment, the associated electric and magnetic fields can be determined. Using the superposition of the fields of all segments, the resulting electric field $\mathbf{E}$ and the magnetic field $\mathbf{H}$ at arbitrary points can be calculated. A detailed description of this procedure is given in [5] or [12]. Introducing the electric and magnetic field model $\mathbf{\Psi}_\mathrm{EI}$ and $\mathbf{\Psi}_\mathrm{HI}$, the relation between the current distribution and the electromagnetic field is given:

$$[\mathbf{E}^\mathrm{T} \quad \mathbf{H}^\mathrm{T}]^\mathrm{T} = [\mathbf{\Psi}_\mathrm{EI}^\mathrm{T} \quad \mathbf{\Psi}_\mathrm{HI}^\mathrm{T}]^\mathrm{T} \cdot \mathbf{I}_\mathrm{S} . \tag{2}$$

According to [12] a dipole model is used for the magnetic field. As presented in [5], the electric field is described by the solution of quasi-static field equations.

Based on (1) and (2), the inverse problem could be formulated. However, as presented in [5], the scaling factors α_E and α_H are introduced to normalize the different orders of magnitudes and units of the electric and magnetic field. These factors are chosen as reciprocal of the Euclidean norm of the field data vectors $\mathbf{E}$ and $\mathbf{H}$. According to the size M of the vectors $\mathbf{E}$ and $\mathbf{H}$, the scaling matrix $\mathbf{\Psi}_\mathrm{s}$ is defined according to (3), where $\mathbf{I}_\mathrm{M}$ is the identity matrix:

$$\mathbf{\Psi}_\mathrm{s} = \begin{bmatrix} \alpha_\mathrm{E}\mathbf{I}_\mathrm{M} & \mathbf{0} \\ \mathbf{0} & \alpha_\mathrm{H}\mathbf{I}_\mathrm{M} \end{bmatrix}, \quad \alpha_\mathrm{E} = \frac{1}{\|\mathbf{E}\|}, \quad \alpha_\mathrm{H} = \frac{1}{\|\mathbf{H}\|} . \tag{3}$$

Finally, introducing the scaled field data $\mathbf{F}$ and the matrix $\mathbf{\Psi}$, the inverse problem is given:

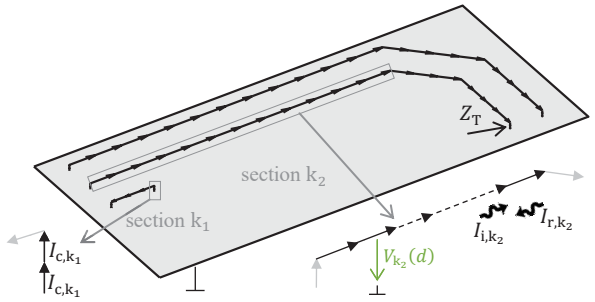

Fig. 1. Schematic presentation of the discretization of a trace system into segments with their currents and voltages, the generated near-field, and an exemplary termination Z_T.

$$\underbrace{\mathbf{\Psi}_\mathrm{s} \cdot [\mathbf{E}^\mathrm{T} \quad \mathbf{H}^\mathrm{T}]^\mathrm{T}}_{=\mathbf{F}} = \underbrace{\mathbf{\Psi}_\mathrm{s} \cdot [\mathbf{\Psi}_\mathrm{EI}^\mathrm{T} \quad \mathbf{\Psi}_\mathrm{HI}^\mathrm{T}]^\mathrm{T} \cdot \mathbf{\Psi}_\mathrm{TL}}_{=\mathbf{\Psi}} \cdot \mathbf{I} \tag{4}$$

In addition, constraints based on the continuity of current and voltage at transitions of sections are introduced. As presented in [13] an equation system using the matrix $\mathbf{K}_\mathrm{C}$ is formulated:

$$\mathbf{K}_\mathrm{C} \cdot \mathbf{I} = \mathbf{0} . \tag{5}$$

Besides, if it is known that a termination is passive, then this a priori knowledge can be represented in an additional nonlinear constraint [5]. E.g., if the termination impedance Z_T in Fig. 1 is passive, the condition must be met [5]:

$$\left|I_{\mathrm{i,k}_2}\right| \leq \left|I_{\mathrm{r,k}_2}\right| . \tag{6}$$

B. Iterative Algorithm for Current Reconstruction

Generally, the inverse problem is solved by a least square approach. If phase information is unknown, then the iterative algorithm presented in [13] is used. First, the scaled magnitudes of the measured field data $|\mathbf{F}^{[0]}|$ are combined with an initial guess of the phase distribution $\boldsymbol{\varphi}^{[0]}$. As presented in [13], a random uniform distribution phase in the range of $[0,2\pi]$ is used in this paper. Thus, the initial field data are given by:

$$\mathbf{F}^{[0]} = \left|\mathbf{F}^{[0]}\right| \circ \exp\left(\mathrm{j}\, \boldsymbol{\varphi}^{[0]}\right) . \tag{7}$$

Here, the Hadamard product ($\circ$) represents an element-wise product. Now, in the i-th iteration step, a current distribution is estimated:

$$\hat{\mathbf{I}}^{[i]} = \arg\min_{\tilde{\mathbf{I}}} \left\| \mathbf{\Psi} \cdot \tilde{\mathbf{I}} - \mathbf{F}^{[i]} \right\|_2^2 , \qquad i \in \mathbb{N} . \tag{8}$$

Here, the constraints presented in (5) or (6) can be considered. Based on this estimated current distribution, the complex-valued near-field $\hat{\mathbf{F}}^{[i]}$ is approximated:

$$\hat{\mathbf{F}}^{[i]} = \mathbf{\Psi} \cdot \hat{\mathbf{I}}^{[i]}, \qquad i \in \mathbb{N}. \tag{9}$$

Its phase information is used to formulate the complex-valued field data for the next iteration step:

$$\mathbf{F}^{[i+1]} = \left|\mathbf{F}^{[0]}\right| \circ \exp\left(\mathrm{j} \arg \hat{\mathbf{F}}^{[i]}\right), \qquad i \in \mathbb{N}. \tag{10}$$

In [5] or [13], two criteria are defined to formulate a stop condition for the iterative algorithm. One is the mean relative deviation of the estimated current distribution $\hat{\mathbf{I}}^{[i]}$. According to the number of entries $\mathrm{K_I}$ in $\hat{\mathbf{I}}^{[i]}$, this criterion is defined as:

$$\sigma_{\Delta\mathrm{I}}^{[i]} = \frac{1}{\mathrm{K_I}} \sum_{k=1}^{\mathrm{K_I}} \frac{\left|\hat{I}_k^{[i]} - \hat{I}_k^{[i-1]}\right|}{\left|\hat{I}_k^{[i]}\right|} , \qquad \hat{\mathbf{I}}^{[i]} = \left[\hat{I}_1^{[i]} \ \cdots \ \hat{I}_{\mathrm{K_I}}^{[i]}\right]^\mathrm{T}, \quad i \in \mathbb{N}^* . \tag{11}$$

In addition, the mean absolute value of the minimal deviation of the reconstructed phase information for the field data is used. Using $\mathrm{K_F}$ as length of $\hat{\mathbf{F}}^{[i]}$, this criterion is given as:

$$\sigma_{\Delta\varphi}^{[i]} = \frac{1}{\mathrm{K_F}} \sum_{k=1}^{\mathrm{K_F}} \min\left\{\left|\Delta\varphi_k^{[i]}\right|, 2\pi - \left|\varphi_k^{[i]}\right|\right\}, \qquad \arg \hat{\mathbf{F}}^{[i]} - \arg \hat{\mathbf{F}}^{[i-1]} = \left[\Delta\varphi_1^{[i]} \cdots \Delta\varphi_{\mathrm{K_F}}^{[i]}\right]^\mathrm{T}, \quad i \in \mathbb{N}^* . \tag{12}$$

As presented in [8]-[10], the relative error of the approximated $\hat{\mathbf{F}}^{[i]}$ is also introduced:

$$\sigma_\mathrm{F}^{[i]} = \sqrt{\frac{|\mathbf{F}^{[0]}|^\mathrm{T}|\mathbf{F}^{[0]}| - \left|\hat{\mathbf{F}}^{[i]}\right|^\mathrm{T}\left|\hat{\mathbf{F}}^{[i]}\right|}{|\mathbf{F}^{[0]}|^\mathrm{T}|\mathbf{F}^{[0]}|}} , i \in \mathbb{N} . \tag{13}$$

C. Reconstruction of Voltage Distribution and Impedances

Based on the reconstructed current distributions, other values can be found. Using the wave impedance Z_0 of a section described by the transmission line theory, the voltage distribution can be estimated along this section. For example, in section k_2 shown in Fig. 1, the voltage value at position d is given as follows [14]:

$$V_{\mathrm{k}_2}(d) = \mathrm{Z}_{0,\mathrm{k}_2}[\mathrm{e}^{-\gamma_{\mathrm{k}_2} d} \quad \mathrm{e}^{\gamma_{\mathrm{k}_2} d}] \cdot [I_{\mathrm{i},\mathrm{k}_2} \quad I_{\mathrm{r},\mathrm{k}_2}]^{\mathrm{T}} . \qquad (14)$$

Evaluating the current and voltage at the begin or end of a section, the input or termination impedance can be estimated.

III. Conditions for a Successful Reconstruction

In this chapter, the choice of initial conditions, iterations steps, and nonlinear constraints of the iterative algorithm are discussed regarding the influence of the reconstruction results. Moreover, also the influence of noise, frequency, and termination impedance of the trace is investigated. To evaluate the quality of the results, the reconstructed current distribution given in $\mathbf{I}_\mathrm{S}$ or $\mathbf{I}$ could be examined. Since these vectors have several entries, examination is very complex. As presented in [14], the shape of the current distribution along a transmission line is completely described by the propagation constant, wave impedance and termination. Since the propagation and wave impedance are assumed to be known, the reconstructed termination impedance represents the shape of the current distribution in a single value. Therefore, in this chapter, the termination impedance Z_T is used to evaluate the quality of the reconstruction results.

A. Setup for Investigation

The near-field data from a single homogeneous PCB trace approximated by cylindrical wire is evaluated in this chapter. The wire (radius $R = 0.1$ mm, height $h = 2$ mm over ideal ground plane, length $\mathcal{L} = 10$ cm) is perfectly conducting and surrounded by vacuum. Its wave impedance Z_0 is 221 Ω. The wire is terminated with an ideal voltage source (1 V) and the impedance Z_T. The near-field is simulated in CONCEPT-II [15]. For the reconstruction, the magnetic field (parallel to ground plane and perpendicular to the wire) and the electric field (perpendicular to the ground plane) are evaluated at 17 field points over the wire. The field points have a distance of 5 mm to ground. The field points are positioned uniformly distributed between positions 1 ... 9 cm along the wire.

B. Parameters of the Iterative Algorithm

The parameters of the iterative algorithm are discussed now. Firstly, the usage of the nonlinear constraint (6) to enforce passive behavior of terminations is discussed. Secondly, the influence of the initial value and the iteration steps to the solution is investigated. For the investigations presented here, the wire is terminated by $Z_\mathrm{T} = 50\ \Omega$ and the frequency is 10 MHz.

The current reconstruction method is applied in two ways: with and without the use of the nonlinear constraint (6). For both ways, the solutions after 100 and 10,000 iteration steps are investigated. Therefore, the four approaches listed in table I are discussed. The iterative algorithm is applied 100 times for every approach. For each execution, a new random initial phase distribution $\boldsymbol{\varphi}^{[0]}$ is used. Formulas (11)-(13) are calculated for each iteration step and the results are shown in Fig. 2. In Fig. 3, the found termination impedances $\hat{Z}_\mathrm{T}$ are shown. For a more detailed analysis of the results, the results are divided into three groups listed in table II according to the phase of $\hat{Z}_\mathrm{T}$. The several solutions in Fig. 2 and Fig. 3 are colored according to these groups. In table I, the number of solutions in each group is listed. Besides, the computation time is given.

In Fig. 2, a generally descending character of the introduced criteria is observable. Only for $\sigma_{\Delta\mathrm{I}}^{[i]}$ and $\sigma_{\Delta\varphi}^{[i]}$ a temporary increasing behavior is visible in the range of about 10^3 iteration steps for some evaluations. Furthermore, in approach 2 and 4, discontinuous curve shapes of $\sigma_{\Delta\mathrm{I}}^{[i]}$ and $\sigma_{\Delta\varphi}^{[i]}$ can be seen for some evaluations. This can be explained by the usage of the nonlinear condition. Generally, as presented in Fig. 3, the absolute value of all results is close to the actual impedance value ($50\ \Omega$). However, there are significant differences in the found phases. After 100 iteration steps

TABLE I. Parameters of Evaluation Approaches and Their Result Metric

approach	1	2	3	4
use of nonlin. constraint (6)	no	yes	no	yes
iteration steps	100	100	10^4	10^4
number of solutions in I	43	60	59	100
number of solutions in II	16	40	0	0
number of solutions in III	41	0	41	0
computation time in s	6	181	491	$1.3 \cdot 10^4$

TABLE II. Groups of Solutions

	$\lvert\arg(\hat{Z}_\mathrm{T})\rvert \in$	color	description
I	[0 °, 45 °]	green	Close to real solution.
II	(45 °, 90 °]	yellow	Passive reactive behavior.
III	(90 °, 180 °]	blue	Termination with active behavior.

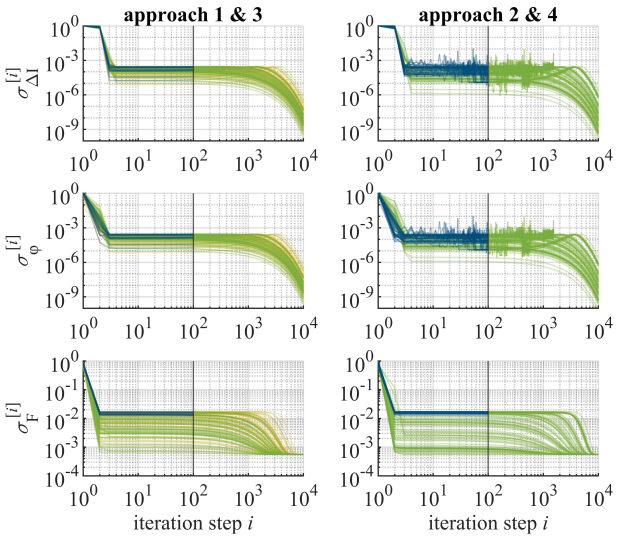

Fig. 2. Development of the criteria (11)-(13) for the evaluation approach according to table I for different initial values.

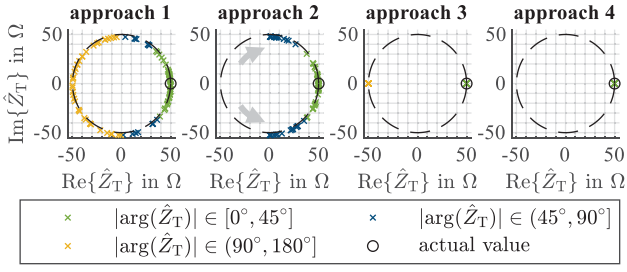

Fig. 3. Estimated values for the termination impedance applying the reconstruction method with the parameters presented in table I for different initial values.

(approach 1 and 2), the phases of the reconstructed termination impedances are widely scattered. Applying 10^4 iteration steps, there is no scattering anymore. While the correct and a wrong value ($\pm 50\ \Omega$) are found in approach 3, in approach 4, only the correct value is found. As expected in approach 2 and 4, all determined termination impedances are passive due to the given constraint. Here, in comparison to the results of approach 1 and 2, a special influence of the constraint on the resulting termination impedance can be observed: A displacement of the estimated phases of the found impedances towards 0. Thereby, a reactive termination (group II) is determined more frequently in approach 2 as in approach 1. However, only for 10^4 iteration steps, the reconstruction results are unique. Here, in approach 4, the a priori knowledge of the passivity of the termination is considered in the calculation of the results. This consideration costs much computation time. In contrast, neglecting the nonlinear constraint (approach 3) reduces the computation time considerably. The a priori knowledge can be applied after the calculation. Correcting the solutions by multiplying (-1), gives nearly the same solutions as in approach 4. Due to the much shorter calculation time, this procedure is recommended and applied in the next investigations. Furthermore, many iteration steps are necessary to get a unique solution. For this purpose, the criteria $\sigma_{\Delta \mathrm{I}}^{[i]}$ and $\sigma_{\Delta \varphi}^{[i]}$ are more practical than $\sigma_{\mathrm{F}}^{[i]}$, as $\sigma_{\mathrm{F}}^{[i]}$ can drop to a very small value even for few iteration steps. The development of the criteria $\sigma_{\Delta \mathrm{I}}^{[i]}$ and $\sigma_{\Delta \varphi}^{[i]}$ are nearly equivalent. So, the formulation of a stop condition using only one of these criteria is recommended.

C. Configuration and Setup Parameters

Now, the parameters of the single wire setup are varied to investigate the influence on a successful reconstruction. Specifically, the influence of frequency, termination impedance and noise are examined.

For these investigations, noise is added to the simulated field data. A normally distributed shift is added to absolute value of the simulated field strength. Using the level σ_{L} (in dB), the noisy scaled field data $\tilde{\mathbf{F}}^{\mathrm{T}} = \left[\tilde{f}_1, \ldots, \tilde{f}_{\mathrm{K_F}}\right]$ are

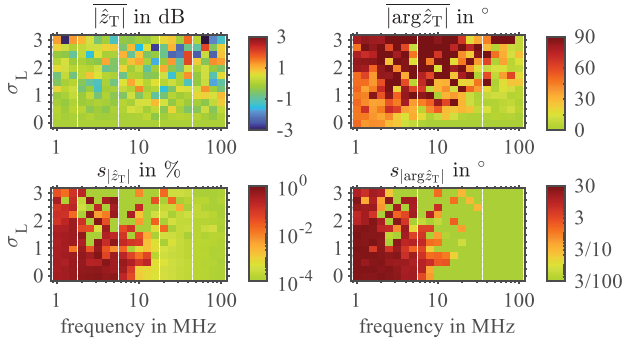

Fig. 4. Mean values $\overline{(\cdot)}$ and standard deviations $s_{(\cdot)}$ of the absolute value and the phase of the estimated termination impedance for $Z_\mathrm{T} = 50\ \Omega$ over frequency for several noise levels.

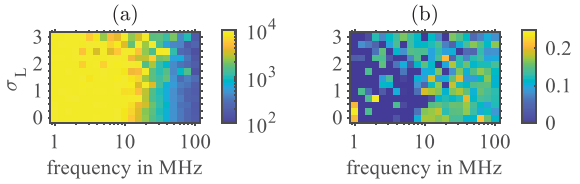

Fig. 5. (a) Mean value and (b) standard deviation normalized to the mean value of the performed iteration steps the setup terminated with $Z_\mathrm{T} = 50\ \Omega$ for several frequencies and noise levels.

determined by the original scaled field data $\mathbf{F}^{\mathrm{T}} = \left[f_1, \ldots, f_{\mathrm{K_F}}\right]$ according to:

$$\tilde{f}_i = f_i \cdot 10^{(\sigma_\mathrm{L} \cdot n)/20}\ \forall\ i \in \mathbb{N}^*_{\leq \mathrm{K_F}}, \qquad n \sim \mathcal{N}(0,1)\,. \tag{15}$$

For the reconstruction, the iterative algorithm is applied 50 times with different initial values for the same noise sample at each frequency. The algorithm is stopped if

$$\sigma_{\Delta \mathrm{I}}^{[i]} \leq 10^{-7} \tag{16}$$

is fulfilled or 10^4 iteration steps are performed. As proposed before, only the linear condition (5) is used. Also, if an active termination behavior is found, the values are corrected. In contrast to the investigation before, the reconstruction results for each frequency are evaluated by mean values and standard deviations. For this, the estimated normalized termination impedance $\hat{z}_\mathrm{T}$ is introduced. This is defined as the relation between the estimated and real impedance:

$$\hat{z}_\mathrm{T} = \frac{\hat{Z}_\mathrm{T}}{Z_\mathrm{T}}\,. \tag{17}$$

The mean $\overline{|\hat{z}_\mathrm{T}|}$ and the standard deviation $s_{|\hat{z}_\mathrm{T}|}$ are used to assess the determined absolute values $|\hat{z}_\mathrm{T}|$. Besides, based on the absolute phase deviation $|\arg \hat{z}_\mathrm{T}|$, the estimated phases are also rated with the mean and the standard deviation.

First, an exemplary evaluation for $Z_\mathrm{T} = 50\ \Omega$ is done in the frequency range from 1 MHz to 100 MHz. The introduced noise model is applied with $\sigma_\mathrm{L} = 0 \ldots 3$ dB. In Fig. 4, the determined mean values and standard deviations are presented. For $\sigma_\mathrm{L} \leq 1$ dB, $\overline{|\hat{z}_\mathrm{T}|}$ is close to the actual value for each frequency. No significant dependence on the frequency can be found. Only for $\sigma_\mathrm{L} \geq 1$ dB and higher frequencies, higher deviations occur. In contrast, a dependency on the frequency of $|\arg \hat{z}_\mathrm{T}|$ can be observed. For higher frequencies, a decreasing error can be observed. As observed for $\overline{|\hat{z}_\mathrm{T}|}$, higher deviations of $|\arg \hat{z}_\mathrm{T}|$ occur for $\sigma_\mathrm{L} \geq 1$ dB. Here, the small number of 17 field measurement points used for the reconstruction might be the reason for the deviations. Using more data points, a more robust evaluation can be assumed. The standard deviations depend on the frequency too. Above 10 MHz the standard deviations drop almost abruptly. These drops are nearly independent for $\sigma_\mathrm{L} \leq 1.5$ dB. For higher noise levels, such drops are already observable for lower frequencies. Representative for both standard deviations, the values of $s_{|\arg \hat{z}_\mathrm{T}|}$ are analyzed in more detail. Since wrongly estimated active terminations are corrected, an absolute phase deviation in the range of $[0, 90\ °]$ is possible. Thus, a standard deviation of about $30\ °$ is a significant marker for wide scattering, while a value below $0.3\ °$ indicates neglectable scattering. Therefore, the standard deviation is proposed as indicator for a unique reconstruction.

In Fig. 5, the mean value and the standard deviation of the performed iteration steps are presented. Here, the standard deviation is normalized to the mean value. Generally, the performed iteration steps are independent to the noise level. For low frequencies, if a unique reconstruction is not possible, the iteration is predominantly terminated by the fact that the maximum possible steps have been performed. In the other cases, condition (16) is met, a unique reconstruction can be achieved after 100 to 1000 iteration steps. Thereby, the scattering of the iteration steps is less than 20 %.

Based on the observations of Fig. 4 and Fig. 5, the iterative algorithm quickly finds unique results above a specific

frequency. This can be explained by the occurrence of wave phenomena in the current distributions. For lower frequencies, the current is nearly constant. Due to model errors or numerical inaccuracy, the reconstructions are not successful here.

Now, the dependence of the termination impedance for a unique reconstruction is investigated. Here, only the standard deviation of the absolute phase deviation is evaluated. Since in the previous investigation the reconstructability has been independent from the noise level, $\sigma_{\mathrm{L}} = 0$ is chosen. Again, the setup is analyzed in the frequency range from 1 MHz to 100 MHz and the iterative algorithm is applied 50 times on the same noise sample at each frequency. In contrast to the investigation before, the frequency is represented as quotient of wire length $\mathcal{L}$ and wavelength λ. Also, the termination impedance is varied from 2.2 Ω to 22 kΩ (respective $Z_0/100$ to $Z_0 \cdot 100$). In Fig. 6, the evaluated standard deviations of the absolute phase deviation are presented. As in the previous investigation, an abrupt drop to a very low standard deviation above a specific frequency is observed for each impedance value. Considering a low value of the standard deviation as an indicator for an unambiguous reconstruction, the symmetric dependence on the termination impedance is impressive. With significant reflections due to a mismatched termination, an unambiguous reconstruction is possible even at lower frequencies. Based on the computed data, the inequation

$$\frac{\mathcal{L}}{\lambda} > 0.0106 \cdot \begin{cases} (Z_0/Z_{\mathrm{T}})^{0.901} & , Z_0/Z_{\mathrm{T}} < 1 \\ (Z_{\mathrm{T}}/Z_0)^{0.901} & , Z_{\mathrm{T}}/Z_0 \leq 1 \end{cases} \tag{18}$$

can be found, which gives calculation errors of less than 1 °. Thus, for an unknown termination, an unambiguous reconstruction would be possible for $\mathcal{L}/\lambda \gtrsim 1/100$ (about $f \gtrsim 30$ MHz for the analyzed structure).

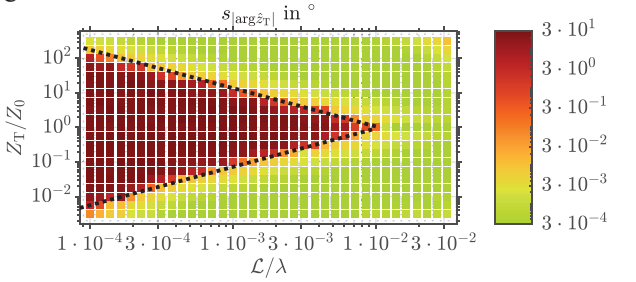

Fig. 6. Determined sample standard deviation of $|\arg \hat{z}_{\mathrm{T}}|$ in the reconstruction for several frequencies and termination impedances. Limit value of (18) is shown as dotted line.

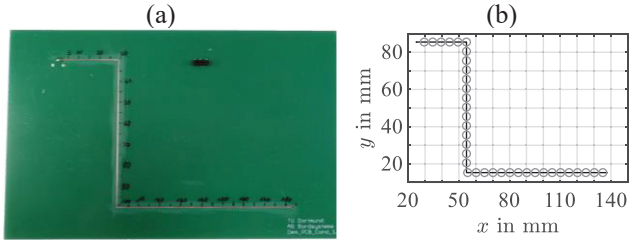

Fig. 7. (a) Photography of the investigated PCB and (b) schematic presentation of the PCB's trace and the measurement points.

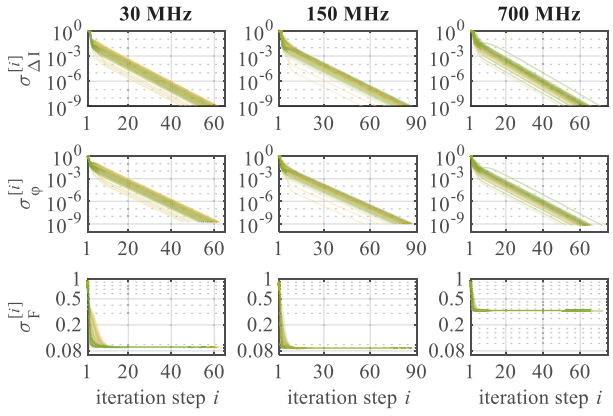

Fig. 8. Development of the criteria (11)-(13) for the 100 evaluations of the measured data.

IV. Applications to Measurement Data

Now the method is applied to the measured data from a simplified PCB with a single trace shown in Fig. 7. The trace has a width of 0.55 mm, thickness of 35 µm, and height above ground plane of 1.55 mm. Assuming a relative permittivity of 4.7 for the substrate, a wave impedance of 105 Ω and an effective relative permittivity of 3.2 are calculated according to [16]. The complete length of the trace is $\mathcal{L} = 183$ mm. At $l = \mathcal{L}$, the trace is terminated by 11 Ω.

As measurement device, a network analyzer KEYSIGHT (AGILENT) E5071B is used. The trace is powered at $l = 0$. For the field measurement, the magnetic field probe RF-R 3-2 from LANGER EMV and the electric field probe RS-E 10 from RHODE & SCHWARZ are used and directly connected to the network analyzer. For the determination of the probe factors, a reduced CONCEPT-II-simulation model is used. Constructed with inhomogeneous media and a round wire, this simulation represents the first section of the trace ($l \in [0{,}30$ mm$]$). In Fig. 7(b) the field measurement points are shown. All 36 measurement points are 3 mm above the trace (4.5 mm above ground plane). The uncertainty of the positioning is 1 mm. The field components H_x, H_y and E_z are measured. For one component, the measurement time is 9 min 35 sec with the applied near-field scanner system. Additionally, the voltage distribution along the trace is measured manually with a LANGER EMV HFU 02 probe at 38 points (measurement time approx. 10 min). The measurement data are scaled to the voltage of $(1 + \mathrm{j}0)$ V at $l = 0$.

In the reconstruction model, the segment length is 0.5 mm for the vertical sections and about 1 mm for the horizontal parts. Only considering the linear constraint, the iterative algorithm is applied to evaluate the phase-less near-field data. It is applied 100 times different initial values, and stopped each time if

$$\sigma_{\Delta \mathrm{I}}^{[i]} \leq 10^{-9} \tag{19}$$

is fulfilled. Here, the results for several exemplary frequencies are discussed. As before, the solutions are colored according to the groups in table II.

The results (11)-(13) of the iteration process are presented in Fig. 8. As discussed before, for $\sigma_{\Delta \mathrm{I}}^{[i]}$ and $\sigma_{\Delta \varphi}^{[i]}$, nearly the same developments are observable. However, an early convergence of $\sigma_{\mathrm{F}}^{[i]}$ is noticeable. This is explainable by deviations of the measurement setup and data to the reconstruction model. As shown before, the $\sigma_{\Delta \mathrm{I}}^{[i]}$ and $\sigma_{\Delta \varphi}^{[i]}$ are more useful than $\sigma_{\mathrm{F}}^{[i]}$ to formulate a stop condition.

In Fig. 9, the reconstructed current and voltage distributions are presented. The phases are shifted to match to the reference phases of the voltages at $l = 0$. Furthermore, the measured voltage distributions and the analytic solution using

the transmission line theory are shown. For all presented frequencies, unambiguous solutions for the magnitude are found. Two solutions for the phase information can be found. As expected, these solutions differ in their implication of a passive or active termination. The reconstructed values are close to the real currents. The small deviations are probably caused by wrong material parameters, uncertainties in the probe position and the used probes factors.

V. Conclusion and Outlook

In this paper, approaches and parameters for a successful reconstruction of currents, voltages and termination impedances of PCB traces are discussed. Input data are phase-less measured E- and H-field distributions. Applying an iterative algorithm, solutions independently from a chosen initial value can be found.

Different criterions to formulate stop conditions are investigated, and a promising condition could be proposed. In addition, conditions for a successful reconstruction about the investigated structure are also determined. Depending on the wave impedance and the termination impedance, the trace-length-to-wave-length-ratio must be large enough. Mismatched terminated traces give accurate results already for lower trace-length-to-wave-length-ratios than matching terminations. Finally, the findings are used for the reconstruction based on measured near-field data of a PCB trace. The current and voltage distributions could be reconstructed with good accuracy for a set of investigated frequencies.

Using the presented method for the investigation of EMI sources, we expect to get more accurate results. More complex PCB structures will be investigated in future and the presented method should be enhanced based on multi-transmission line theory to investigate coupled traces.

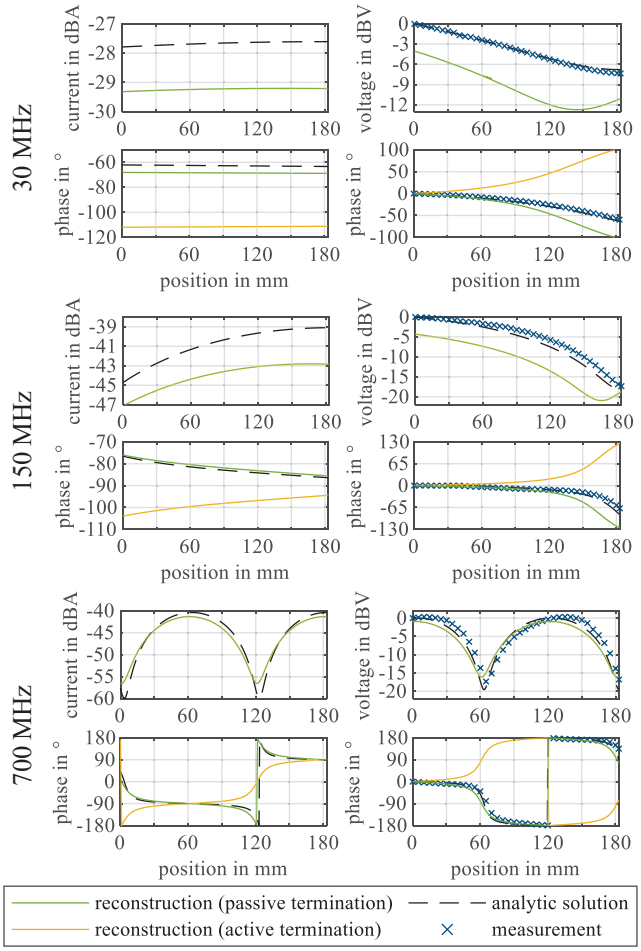

Fig. 9. Reconstructed current and voltage distributions based on measured near-field data for several exemplary frequencies.

References

[1] X. Gao, J. Fan, Y. Zhang, H. Kajbaf, and D. Pommerenke, "Far-Field Prediction Using Only Magnetic Near-Field Scanning for EMI Test," *IEEE Trans. Electromagn. Compat.*, vol. 56, no. 6, pp. 1335–1343, May 2014, doi: 10.1109/TEMC.2014.2322081.

[2] H. Rezaei *et al.*, "Source Reconstruction in Near-Field Scanning Using Inverse MoM for RFI Application," *IEEE Trans. Electromagn. Compat.*, vol. 62, no. 4, pp. 1628–1636, Jan. 2020, doi: 10.1109/TEMC.2020.3006031.

[3] Y. Vives-Gilabert, C. Arcambal, A. Louis, F. Daran, P. Eudeline, and B. Mazari, "Modeling Magnetic Radiations of Electronic Circuits Using Near-Field Scanning Method," *IEEE Trans. Electromagn. Compat.*, vol. 49, no. 2, pp. 391–400, Jan. 2007, doi: 10.1109/TEMC.2006.890168.

[4] P. Maheshwari, H. Kajbaf, V. V. Khilkevich, and D. Pommerenke, "Emission Source Microscopy Technique for EMI Source Localization," *IEEE Trans. Electromagn. Compat.*, vol. 58, no. 3, pp. 729–737, Jan. 2016, doi: 10.1109/TEMC.2016.2524594.

[5] R. Nowak, A. Henke, and S. Frei, "Characterization of EMI Sources from Reconstructed Current Distributions Based on Phase-Less Electric and Magnetic Near-Field Data," in *2020 International Symposium on Electromagnetic Compatibility - EMC EUROPE*, 2020, Rome, Italy, doi: 10.1109/EMCEUROPE48519.2020.9245636.

[6] H. Zhao, Y. Zhang, J. Hu, and E.-P. Li, "Iteration-Free-Phase Retrieval for Directive Radiators Using Field Amplitudes on Two Closely Separated Observation Planes," *IEEE Trans. Electromagn. Compat.*, vol. 58, no. 2, pp. 607–610, Jan. 2016, doi: 10.1109/TEMC.2015.2514111.

[7] M. Johansson, A. Fhager, H.-S. Lui, and M. Persson, "Comparison Between Two Phase-Retrieval Methods for Electromagnetic Source Modeling," *Prog. Electromagn. Res. B*, vol. 30, pp. 239–253, Jan. 2011, doi: 10.2528/PIERB11020507.

[8] J. Zhang and J. Fan, "Source Reconstruction for IC Radiated Emissions Based on Magnitude-Only Near-Field Scanning," *IEEE Trans. Electromagn. Compat.*, vol. 59, no. 2, pp. 557–566, Jan. 2017, doi: 10.1109/TEMC.2016.2638760.

[9] Y.-F. Shu, X.-C. Wei, R. Yang, and E.-X. Liu, "An Iterative Approach for EMI Source Reconstruction Based on Phaseless and Single-Plane Near-Field Scanning," *IEEE Trans. Electromagn. Compat.*, vol. 60, no. 4, pp. 937–944, Jan. 2018, doi: 10.1109/TEMC.2017.2756902.

[10] L. Wang, Y. Zhang, F. Han, J. Zhou, and Q. H. Liu, "A Phaseless Inverse Source Method (PISM) Based on Near-Field Scanning for Radiation Diagnosis and Prediction of PCBs," *IEEE Trans. Microw. Theory Tech.*, vol. 68, no. 10, pp. 4151–4160, Jan. 2020, doi: 10.1109/TMTT.2020.3006564.

[11] T.-H. Song, X.-C. Wei, Z.-Y. Tang, and R. X.-K. Gao, "Broadband Radiation Source Reconstruction Based on Phaseless Magnetic Near-Field Scanning," *IEEE Antennas Wirel. Propag. Lett.*, vol. 20, no. 1, pp. 113–117, Jan. 2021, doi: 10.1109/LAWP.2020.3042538.

[12] R. Nowak and S. Frei, "Reconstruction of Current Distribution and Termination Impedances of PCB-Traces by Magnetic Near-Field Data and Transmission-Line Theory," in *2018 International Symposium on Electromagnetic Compatibility - EMC EUROPE*, 2018, Amsterdam, The Netherlands, doi: 10.1109/EMCEurope.2018.8485103.

[13] R. Nowak and S. Frei, "Reconstruction of Current Distribution on a Given Conductor Structure Using Frequency Domain Near-Field Data without Phase Information," in *2019 International Symposium on Electromagnetic Compatibility - EMC EUROPE*, 2019, Barcelona, Spain, doi: 10.1109/EMCEurope.2019.8872074.

[14] C. R. Paul, *Analysis of multiconductor transmission lines*, 2. ed. Piscataway, NJ: IEEE Press, 2008.

[15] H.-D. Brüns. *CONCEPT-II*. (2020). Hamburg University of Technology. [Online]. Available: http://www.tet.tuhh.de/concept/

[16] T. C. Edwards and M. B. Steer, *Foundations for microstrip circuit design*, Fourth edition. Chichester: Wiley IEEE, 2016.